Direct-Drive, Active Compliant End-Effector
(Active RCC)

H. Kazerooni
J. Guo

Mechanical Engineering Department
University of Minnesota
Minneapolis, MN 55455

Abstract

The design and construction of a fast, light-weight, active end-effector which can be attached to the end-point of a commercial robot manipulator is presented here. Electronic compliancy (Impedance Control) (11) has been developed on this device The end-effector behaves dynamically as a two-dimensional, Remote Center Compliance (RCC). The compliancy in this active end-effector is developed electronically and can therefore be modulated by an on-line computer. The device is a planar, five-bar linkage which is driven by two direct drive, brush-less DC motors. A two-dimensional, piezoelectric force cell on the end-point of the device, two 12-bit encoders, and two tachometers on the motors form the measurement system for this device. The high structural stiffness and light weight of the material used in the system allows for a 25 Hertz bandwidth Impedance Control.

Nomenclature

E	environment dynamics
e	input trajectory
f	contact force
G	closed-loop transfer function matrix
H	the compensator
j	complex number notation $\sqrt{-1}$
J_e	Jacobian
J_i	moment of inertia of each link relative to the end-point of the link
K	stiffness matrix
K_n , K_t	stiffness in the direction normal and tangential to the part
l_i , m_i	length and mass of each link
M_o	inertia matrix
M	the grinder mass in the passive end-effector
S	sensitivity transfer function matrix
r	input command vector
$T=[T_1\ T_2]^T$	torque vector
$X=[X_t\ X_n]^T$	vector of the tool position in the Cartesian Coordinate frame
X_e	environment position before contact
x_i, θ_i	location of the center of mass and orientation of each link
α	small perturbation of θ_1 in the neighborhood of $\theta_1 = 90°$
δe	end-point deflection in $X_n$direction
δX_n , δX_t	end-point deflection in the direction normal and tangential to the part
δF_n , δF_t	contact force in the direction normal and tangential to the part
ω_b	frequency range of the burr observed from the robot end-point
ω_d	dynamic manipulability
ω_o	frequency range of the operation (bandwidth)
ω_r	frequency range of the robot oscillations

1. Introduction

Manufacturing manipulations require mechanical interaction with the environment or with the object being manipulated. Robot manipulators are subject to interaction forces when they maneuver in a constrained work-space. Inserting a computer board in a slot or deburring an edge are examples of constrained maneuvers. In constrained maneuvers, one is concerned with not only the position of the robot end-point, but also the contact forces. In constrained maneuvering, the interaction forces must be accommodated rather than resisted. If we define compliancy as a measure of the ability of the manipulators to react to interaction forces and torques, the objective is to assure compliant motion (passively or actively) for the robot end-point in the cartesian coordinate frame for manipulators that must maneuver in the constrained environments.

An example of the manufacturing manipulation that requires compliancy is robotic assembly. To perform the assembly of parts that are not perfectly aligned, one must use a compliant element between the part and the robot to ease the insertion process. The RCC is a device that can be attached to the end-point of the robot manipulators (3,20). This device develops a passive compliant interface between the robot and the part. The primary function of the RCC is to act as a filter that decreases the contact force between the part and the robot due to the robot oscillations, robot programming error, and part fixturing errors. These end-effectors are called passive because the elements that generate compliancy are passive and no external energy is flowing into the system.

Active end-effectors are devices that can be mounted at the end-point of the robot manipulators to develop more

degrees of freedom (5). This paper describes the design, construction and control of an active end-effector that can be used as a compliant tool holder. There is no passive compliant element in the system, because the compliancy in the system is generated electronically (6,7,11). The advantage of this system over other passive systems is that one can modulate the compliancy in the system arbitrarily by an on-line computer, depending on the requirements of the tasks. Two DC actuators power the two degrees of freedom of the system.

2. Architecture

Figure 1 shows the schematic diagram of the active end-efector.

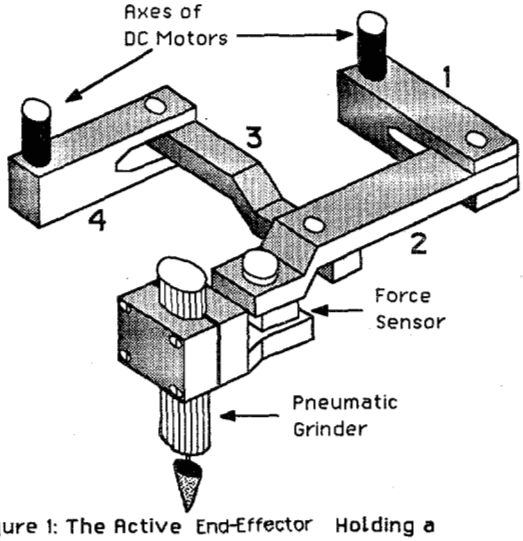

Figure 1: The Active End-Effector Holding a Pneumatic Grinder

The end-effector is a 5-bar linkage with two degrees of freedom. All are articulated drive joints. The links are made of Aluminium 6061. The actuators are DC brush-less direct drive motors equipped with 12 bit encoders and tachometers. The choice of the direct drive system eliminates backlash and develops more structural rigidity in the system. This structural rigidity allows for a wide control bandwidth and higher precision. The stall torque and the peak torque for each motor is 5 lb-in and 20 lb-in, respectively. Each motors weighs 2.4 lbs. A wide-bandwidth piezoelectric based force sensor is located between the end-point of the mechanism and the end-effector gripper to measure the force on the tool. The force sensor is pre-loaded by a clamping bolt, and measures the force in two dimensions in the plane of the mechanism. The entire weight of the links with bearings and force sensor is 111.4 grams. The end-effector can be attached to the robot manipulator by a simple fixture between the housing of the motors and the robot end-point. Figure 2 shows the side view of the end-effector.

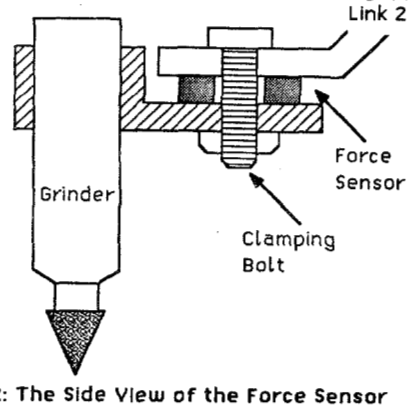

Figure 2: The Side View of the Force Sensor Assembly

The characteristics of this end-effector is as follows:

Size of the 5-bar linkage at nominal position	2.167"×4.160"
The height of the end-effector with motors (excluding the grinder tool)	3.760"
Linear work-space of the end-point	0.3" ×0.3"
Resolution of the end-point motion	2.6×10^{-3} "
Bandwidth of the control system	15 hertz
Total mass of the mechanism (without the tool)	0.25 lb.
Weight of two motors	4.8 lb.
Weight of the tool	0.3 lb.
Total mass (mass of the mechanism and the motors, excluding the grinding tool)	5.05 lb.

Figure 3 shows the size of the end-effector relative to a hand (small hand).

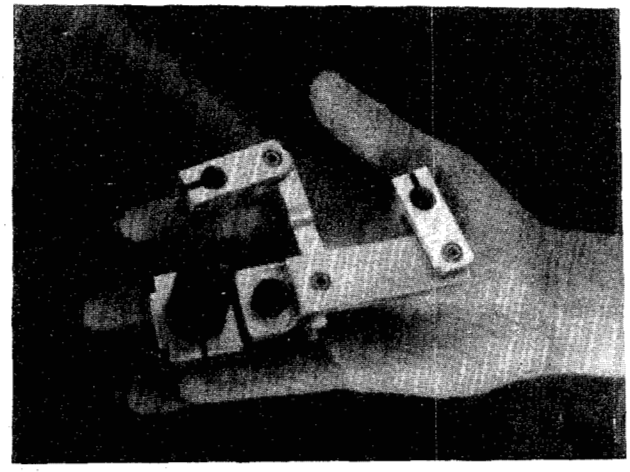

Figure 3: The Active End-Effector

3. Motivation for Development of the Active End-effector

In this section we explain briefly a practical problem that requires modulation of the compliance in the system by an on-line computer. This example also shows the limitation of passive RCC in developing a desired stiffness for arbitrary frequency ranges. The details of the problem is given in references (8,9,10).

Consider the deburring of a surface by a robot manipulator; the objective is to use an end-effector to smooth the surface down to the commanded trajectory depicted by the dashed line in Figure 4. It is intuitive to design a system with a large impedance (small compliance) in the normal direction and a small impedance (large compliance) in the tangential direction. We define impedance as the ratio of the contact force to the end-effector deflection and as a function of frequency.

A large impedance in the normal direction causes the end-point of the grinder to reject the interaction forces and stay very close to the commanded trajectory

(dashed-line). The larger the impedance of the end-effector in the normal direction, the smoother the surface will be. Given the volume of the metal to be removed, the desired tolerance in the normal direction prescribes an approximate value for impedance in the normal direction. The force necessary to cut in the tangential direction at a constant traverse speed is approximately proportional to the volume of the metal to be removed (8,9,10). Therefore, the larger the burrs on the surface, the slower the manipulator must move in the tangential direction to maintain a relatively constant tangential force. This is necessary because the slower speed of the end-point along the surface implies a smaller volume of metal to be removed per unit of time, and consequently, less force in the tangential direction. To remove the metal from the surface , the grinder should slow down in response to contact forces with large burrs.

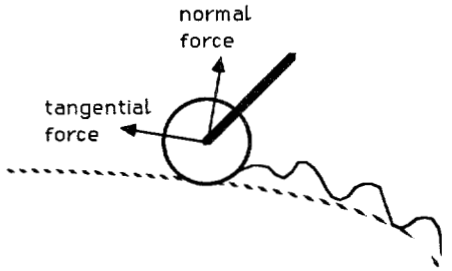

Figure 4: Deburring an Edge

The above explanation demonstrates that it is necessary for the end-effector to accommodate the interaction forces along the tangential direction, which directly implies a small impedance value in the tangential direction. If a designer does not accommodate the interaction forces by specifying a small stiffness value in the tangential direction, the large burrs on the surface will produce large contact forces in that direction which stall the tool. Large contact forces in the tangential direction may develop a deflection in the end-point position in the normal direction, which might exceed the desired tolerance. A small value for the impedance in the tangential direction (relative to the impedance in the normal direction) guarantees small contact force in the tangential direction. The frequency spectrum of the roughness of the surface and the desired translational speed of the robot along the surface determine the *frequency range of operation*, ω_b.

On the other hand, for compensation of the robot oscillation, the impedance of the end-effector in the normal direction must be small for all the frequency range of the robot oscillations and fixturing errors, ω_r. The small impedance (large compliance) in the normal direction allows for compensation of the robot position uncertainties and part fixturing errors. Choosing a large impedance in the normal direction for deburring purpose conflicts with the required impedance to compensate for robot oscillations. The compensation for robot position uncertainties demands a low impedance (large compliance) in the normal direction, while a large impedance is required for deburring purposes. In theory, both requirements could be satisfied if one designs an end-effector with the dynamic characteristics shown in Figure 5. As shown in Figure 5, $|\delta X_n(j\omega)/\delta F_n(j\omega)|$ is very large for all frequency range of the robot oscillations and the fixturing errors, ω_r and very small for all frequency range of the burr, ω_b. While a large $|\delta X_n(j\omega)/\delta F_n(j\omega)|$ in $(0,\omega_r)$ does not let the robot oscillations develop a large variation in the normal contact force, a small $|\delta X_n(j\omega)/\delta F_n(j\omega)|$ in ω_b will cause the end-effector to be very stiff in response to the burrs. Figure 5 also shows the dynamic behavior of the end-effector in the tangential direction. For all $\omega \in \omega_b$, $|\delta X_t(j\omega)/\delta F_t(j\omega)|$ is large to guarantee the deburring requirements. Note that $|\delta X_n(j\omega)/\delta F_n(j\omega)| << |\delta X_t(j\omega)/\delta F_t(j\omega)|$ for all $\omega \in \omega_b$.

It is <u>impossible</u> to design and build a passive end-effector using RCC with the dynamic characteristics shown in Figure 5. This is because of the role the constant mass of the tool plays in the dynamic behavior of the end-effector. Figure 6 shows a passive tool-holder that contains an RCC (2). Since the mass of the grinder is a constant parameter in the dynamic equations of the passive end-effector in both directions, the only possible dynamic behavior for a passive end-effector is of the form given in Figure 6. For a given set of K_n and K_t in both directions, one cannot choose arbitrary natural frequencies (or approximately bandwidth) in both directions. The natural frequencies (or bandwidths) for a passive end-effector are fixed approximately at $\sqrt{K_n/M}$ and $\sqrt{K_t/M}$. Once K_n and K_t are chosen for deburring requirement and the compensation of the robot oscillation and the fixturing errors, then $\sqrt{K_n/M}$ and $\sqrt{K_t/M}$ cannot arbitrarily be chosen to meet the requirements of the ω_r and ω_b. We will show in Section 5 that with active end-effector one can modulate the impedance of the system electronically. This method is called impedance control (4,6,7,11). With this method one can choose arbitrary stiffness in two orthogonal directions, within two various frequency ranges.

4. Design

In this section two significant properties of this end-effector are explained. Although the active end-effector can be used as a micro positioning system for small and fast maneuvering of the tool, it is designed to act as an RCC. The end-point of the end-effector behaves as if there are two orthogonal springs holding the tool.

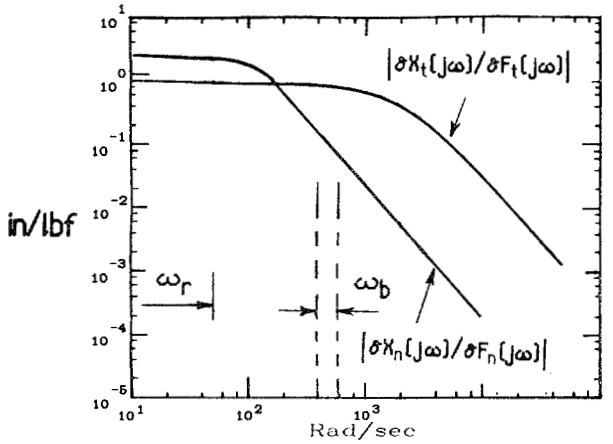

Figure 5: The Required Dynamic Behavior for Deburring

In this behavior, the end-point motion is very small. Equation 1 describes the dynamic behavior of the mechanism, for small perturbation of the mechanism

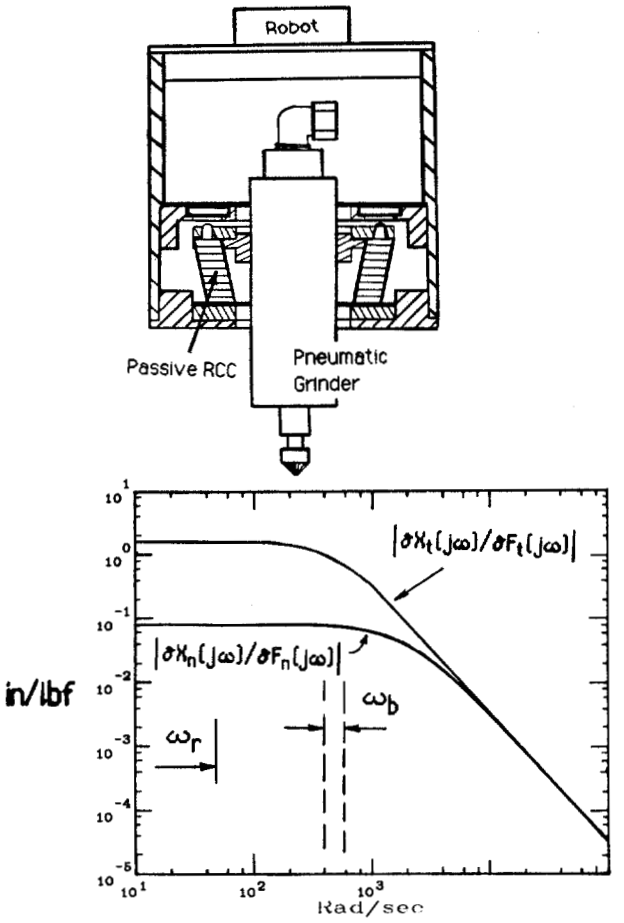

Figure 6: A Passive End-Effector and its Dynamic Behavior (Reference 2)

around its nominal point in absence of the centrifugal and coriolis forces. We will justify the absence of centrifugal and coriolis forces in the dynamic equations of the system in our analysis.

$$\ddot{X} = J_c M_o^{-1} T \qquad (1)$$

Where:

$X = [X_t \;\; X_n]^T$ .....2×1vector of the tool position in the Cartesian Coordinate frame
J_c ..... 2×2 Jacobian matrix
M_o ..... 2×2 mass matrix
$T = [T_1 \;\; T_2]^T$ ..... 2×1 vector of the motor torque

$J_c M_o^{-1}$ is a transmission ratio between the actuator torque and the end-point acceleration. This matrix is function of joint angles. It is desirable to operate the end-effector in an orientation such that $J_c M_o^{-1}$ is almost constant or has minimum rate of change. The general form M_o and J_c are given in Appendix A by equations A1 and A2. Figure A1 in Appendix A shows a five-bar linkage in the general form. The device is designed to operate around the neighborhood of the nominal orientation of $\theta_1 = 90°$, $\theta_2 = 0°$, $\theta_3 = 90°$ and $\theta_4 = 180°$ as shown in Figure 7. θ_1 and θ_4 are the driving angles, and we intend to drive the system such that $85° < \theta_1 < 95°$ and $175° < \theta_4 < 185°$, (Total of ±5° deviation from their nominal values). It can be shown that the rate of change of $J_c M_o^{-1}$ at this nominal orientation is minimum. The dynamic manipulability, ω_d is defined as the square root of the multiplication of the maximum and minimum singular values of $J_c M_o^{-1}$ (19). ω_d measures the rate of change of $J_c M^{-1}$.

$$\omega_d = \sqrt{\sigma_{max}(J_c M_o^{-1})\, \sigma_{min}(J_c M_o^{-1})} \qquad (2)$$

or equivalently:

$$\omega_d = \sqrt{\det(J_c M_o^{-1} M_o^{-T} J_c^T)}$$

ω_d is plotted in Figure 8 as a function of perturbations on $\delta\theta_1$ and $\delta\theta_4$. The perturbation around the nominal values of θ_1 and θ_4 are called $\delta\theta_1$ and $\delta\theta_4$.

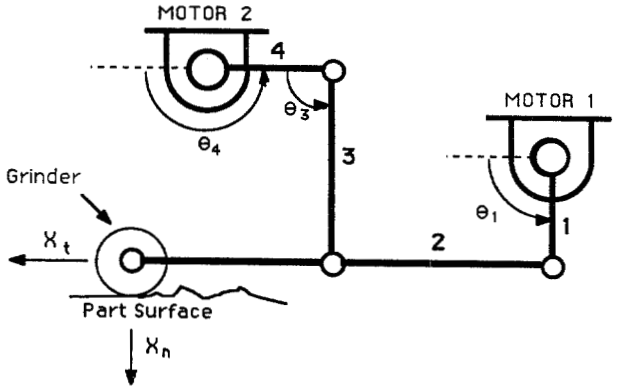

Figure 7: The End-effector at its Nominal Position $\theta_1 = 90°$ and $\theta_4 = 180°$

According to Figure 8, ω_d is "smooth" for all small perturbations around nominal values of θ_1 and θ_4. Inserting $\theta_1 = 90$, $\theta_2 = 0$, $\theta_3 = 90$ and $\theta_4 = 180$ into equations A1 and A2 (from Appendix A) results in diagonal matrices for J_c and M_o such that $J_c M_o^{-1}$ is diagonal and also has the minimum rate of change when θ_1 and θ_4 vary slightly from their nominal values. Note that the plot in Figure 8 shows only that at the configuration shown, $J_c M_o^{-1}$ has the minimum rate of change and this allows us to use equation 1 as our dynamic model for the active end-effector. Since the rate of change of $J_c M_o^{-1}$ is minimum at the nominal configuration, centrifugal and coriolis forces can be neglected from the dynamic equations of the end-effector. (These terms are functions of the rate of change of the inertia matrix). If the end-effector is considered in another configuration, then any slight perturbation of the driving joints will develop significant change in $J_c M_o^{-1}$ and consequently, non-linearity will be developed in the dynamic behavior of the system. Since $J_c M_o^{-1}$ is a diagonal matrix, then the dynamic equation of the end-effector is uncoupled. Based on this uncoupling, for a limited range, motor 1 maneuvers the end-point in X_t-direction, while motor 2 moves the end-point independently in the X_n-direction.

We use the end-effector in the configuration shown in Figure 7. All the links are orthogonal to one another. If θ_1 is perturbed from its nominal value as much as α, then the value of the end-point perturbation in the X_n direction, δe, can be calculated form equation 3. Figure 9 shows the configuration of the perturbed system.

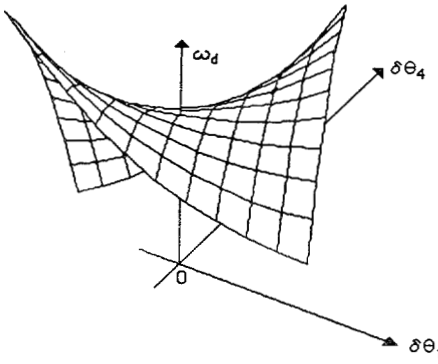

Figure 8: Dynamic Manipulability as a Function of $\delta\Theta_1$ and $\delta\Theta_4$

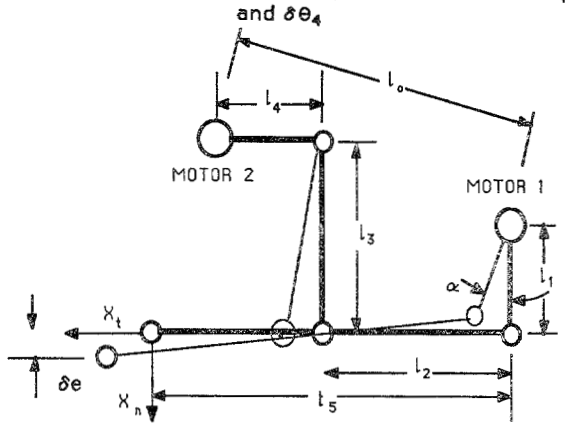

Figure 9 : The 5-bar Mechanism with Small Deflection of α

$$\delta e = \frac{l_1}{2 l_2}\,\alpha^2 \left(l_5 - l_2 - \frac{l_1 l_5}{l_3} \right) \qquad (3)$$

For $\delta e=0$, the following equality must be satisfied.

$$l_5 - l_2 = \frac{l_1 l_5}{l_3} \qquad (4)$$

By satisfying equation 4, we choose the lengths of the mechanism such that the end-point of the end-efector always moves along the X_t axis for small value of α. ($\alpha < \pm 5°$) This configuration is an application of the well known Watts (12). straight line mechanism. This property is attractive for deburring purposes. According to the references (8,10), the end-effector must be very stiff in the direction normal to the part and compliant in the direction tangential to the part. Once the grinder encounters a burr, motor 1, which is responsible for motion in the X_t-direction, moves the tool backward to decrease the amount of the force. In the deburring process, motor 1 constantly moves the end-point back and forth in the X_t-direction. If equation 4 is guaranteed, then the motion of the end-point in the X_t-direction does not affect the motion of the tool in the X_n-direction. The kinematic independence of the end-point motion in X_n-direction from the motion of the end-point in X_t-direction allows for a very smooth surface finish for deburring purposes. The following constraints are sufficient to result in the exact lengths of the mechanism:

- Equation 4 must be satisfied.
- For simplicity in design and construction, $l_1=l_4$ and $l_3=l_2$
- $l_o=3"$ (Each actuator has 1.375" radius)
- l_4 must be such that if $\delta\Theta_4=5°$, the amount of motion in X_n-direction is 0.15".

The above five constraints are sufficient conditions to result the lengths of the five links. Using the triangle equality and some algebra, the following lengths are calculated:

$l_o=3"$, $l_1=0.906"$, $l_2=1.917"$, $l_3=1.917"$ and $l_4=0.906"$

5. Electronic Compliancy

First we frame the controller design objectives by a set of meaningful mathematical terms; then we give a summary of the controller design method to develop compliancy for linear systems. The complete description of the control method to develop electronic compliancy (impedance control) for an n degree of freedom non-linear manipulative system is given in reference 11.

The controller design objective is to provide a stabilizing dynamic compensator for the system such that the ratio of the position of end-point of the end-effector to an interaction force is constant within a given operating frequency range. (The very general definition is given in references 6 and 7). The above statement can be mathematically expressed by equation 5.

$$\delta F(j\omega) = K\,\delta X(j\omega) \qquad \text{for all } 0<\omega<\omega_o \qquad (5)$$

where:

$\delta F(j\omega)$ = 2×1 vector of the deviation of the interaction forces from their equilibrium value in the global cartesian coordinate frame.

$\delta X(j\omega)$ = 2×1 vector of the deviation of the end-point position from the nominal point in the global cartesian coordinate frame.

K = 2×2 real-valued, non-singular diagonal stiffness matrix with constant members.

ω_o = bandwidth (frequency range of operation)

j = complex number notation, $\sqrt{-1}$

The stiffness matrix is the designer's choice which, depending on the application, contains different values for each direction. By specifying K, the designer governs the behavior of the end-effector in constrained maneuvers. Large elements of the K-matrix imply large interaction forces and torques. Small members of the K-matrix allow for a considerable amount of motion in the end-effector in response to interaction forces. Even though a diagonal stiffness matrix is appealing for the purpose of static uncoupling, the K-matrix in general is not restricted to any structure.

Mechanical systems are not generally responsive to external forces at high frequencies. As the frequency increases, the effect of the feedback disappears gradually, (depending on the type of controller used), until the inertia of the system dominates its overall motion. Therefore, depending on the dynamics of the system, equation 5 may not hold for a wide frequency range. It is necessary to consider the specification of ω_o as the second item of interest. In other words, two independent issues are addressed by equation 5: first, a simple relationship between $\delta F(j\omega)$ and $\delta X(j\omega)$; second, the frequency range of operation, ω_o, such that equation 5 holds true. Besides

choosing an appropriate stiffness matrix, K, and a viable ω_o, a designer must also guarantee the stability of the closed-loop system. In summary, we are looking for a dynamic behavior for the manipulative system that resembles the the dynamic behavior shown in Figure 5.

We consider the architecture of Figure 10 as the closed-loop control system for the end-effector. The detailed description of each operator in Figure 10 is given in reference 11. Since the dynamic behavior of the end-effector in the neighborhood of its operating point is linear, all the operators in Figure 10 are considered transfer function matrices. In the general approach for development of compliancy in reference 11, E, G, H and S are non-linear operators.

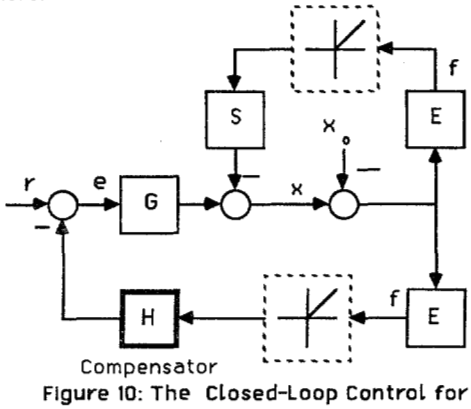

Figure 10: The Closed-Loop Control for the End-Effector

G is the transfer function matrix that represents the dynamic behavior of the manipulative system (end-effector in our case) with a positioning controller. The input to G is a n×1 vector of input trajectory, e. The fact that most manipulative systems have some kind of positioning controllers is the motivation behind our approach. One can use great number of methodologies for the development of the robust positioning controllers (14,15,18) G can be calculated experimentally or analytically. Note that G is approximately equal to the unity matrix for the frequencies within its bandwidth. S is the sensitivity transfer function matrix. S represents the relationship between the external force on the end point of the end-effector and the end-point motion. This motion is due to either structural compliance in the end-effector mechanism or the positioning controller compliance. For good positioning system S is quite "small". (The notion of "small" can be regarded in the singular value sense when S is a transfer function matrix. L_p-norm [18,19] can be considered to show the size of S in the non-linear case.) E represents the dynamic behavior of the environment Readers can be convinced of role of E by analyzing the relationship of the force and displacement of a spring as a simple model of the environment. H is the compensator to be designed. The input to this compensator is the contact force. The compensator output signal is being subtracted from the vector of input command, r, resulting in the error signal, e, as the input trajectory for the robot manipulator r is the input command vector which is used differently for the two categories of maneuverings; as a trajectory command to move the end-point in unconstrained space and as a command to shape the contact force in the constrained space. When the manipulative system and environment are in contact, then the value of the contact force and the end-point position of the robot are given by equations 6 and 7.

$$f=E(I+SE+GHE)^{-1}Gr \tag{6}$$

$$y=(I+SE+GHE)^{-1}Gr \tag{7}$$

The general goal is to choose a class of compensator, H, to shape the impedance of the system, $E(I+SE+GHE)^{-1}G$, in equation 6. When the system is not in contact with the environment, the actual position of the end-point is equal to the input trajectory command within the bandwidth of G. (Note that G is approximately equal to unity matrix within its bandwidth.) When the system is in contact with the environment, then the contact force follows r according to equation 6. The input command vector, r, is used differently for the two categories of maneuverings; as an input trajectory command in unconstrained space and as a command to control force in constrained space. We do not command any set-point for force as we do in admittance control (13,21). This method is called Impedance Control (4,6,7) because it accepts a position vector as input and it reflects a force vector as output. There is no hardware or software switch in the control system when the robot travels from unconstrained space to constrained space. The feedback loop on the contact force closes naturally when the robot encounters the environment. When the system is contact with the environment, then the contact force is is a function of r according to equation 6. This compensator must also guarantee the stability of the system.

We are interested in a particular case when r=0. Suppose the environment is being moved into the end-effector or the end-effector is being moved into the environment. This is the case that occurs in robotic deburring. The relation between the contact force and the end-point deflection is given by equation 8 if E approaches ∞ in the singular value sense. (This is shown in reference 11)

$$f=(S+H)^{-1}x \tag{8}$$

Equality 8 is derived by inspection of the block diagram in Figure 10. The fact that in most manufacturing tasks such as robotic deburring, the end point of the system is in contact with a very stiff environment, is the motivation behind our consideration in development of equation 8. $(S+H)^{-1}$ is similar to the stiffness matrix, K which is defined by equation 5. By selecting the value of H and knowledge of S one can select the members of H such that $(S+H)^{-1}$ of equation 8 meets the deburring requirements as given by equation 5.

6. Experiments

Two sets of experiments are described here to describe the dynamic behavior of the end-effector in constrained and unconstrained maneuverings.

In Section 6.1 the experimental frequency response of the transfer function matrix, G, and the sensitivity transfer function matrix, S are given. The values of G and S are necessary to estimate the stability bound on H. Section 6.2 demonstrates the end-point impedance, $(S+H)^{-1}$ and the uncoupled time-domain closed-loop dynamic behavior of the end-effector in the constrained and unconstrained maneuverings. The control architecture of Figure 10 is used to control the system.

Two brush-less DC motors are used to power the two degrees of freedom of the end-effector. The continuous stall torque and peak torque are 5 lbf-in and 20 lbf-in at 2.25 and 6.7 amp, respectively. Motors are driven by two PWM amplifiers. The amplifier has 7.5 amps continuous output current. Both motors are equipped with resolvers that provide 12-bit orientation data and an analog velocity feedback signal with resolution of 0.019 volts/rad/sec. A 3-component piezoelectric force transducer and a charge amplifier are used to measure forces in two directions in the cartesian coordinate frame. The force transducer is pre-loaded at the end point of the end effector by a clamping screw as shown in Figure 2. The resolution of the force transducer is 2.2×10^{-3} lbf. The stiffness of the force transducer in each measuring direction is about 1.5×10^{9} lbf/in.

Since the dynamic behavior of the end-effector in two directions are uncoupled, matrices E, S , G and H of Figure 10 are diagonal. Each motor of the end-effector was treated separately and a control loop similar to the one in Figure 10 was designed for each motor.

6.1. Experimental and Theoretical Values of G and S

In this set of experiments, the position transfer function matrix, G, the sensitivity transfer function, S are measured. Figure 11 shows the analytical and experimental values of G for two orthogonal directions. For measuring G, a series of sinusoidal commands with frequencies within 25 hertz were imposed on each motor. The amplitude of orientation of each motor was measured at each frequency. The ratio of the rotation of the motor to the input command represents the magnitude of G at each frequency.

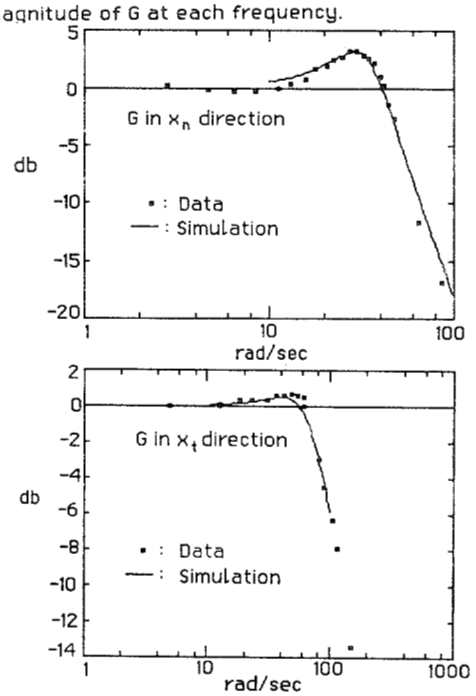

Figure 11 : The Position Transfer Function, G

For measurement of the sensitivity transfer function matrix, the input excitation was supplied by the rotation of an eccentric mass mounted on the tool bit. Figure 12 shows the experimental set-up for measurement of S. The rotating mass exerts a centerifugal sinusoidal force on the tool bit. The frequency of the imposed force is equal to the frequency of rotation of the mass. By varying the frequency of the rotation of the mass, one can vary the frequency of the imposed force on the end-effector. Figure 13 depicts the sensitivity transfer function. The values of the sensitivity transfer functions along the normal and tangential directions, within their bandwidths, are 0.7 in/lbf and 0.197 in/lbf respectively.

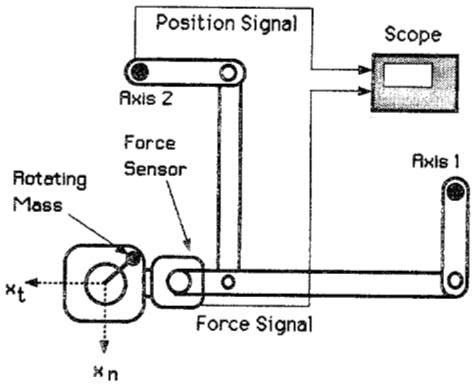

Figure 12: The Experimental Set-up for Measurement of the Sensitivity Transfer Function

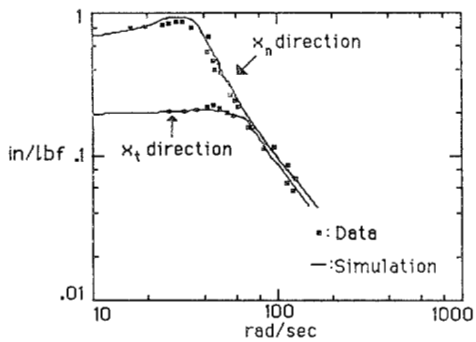

Figure 13: The Sensitivity Transfer Function, S

6.2 The Closed-Loop Dynamic Behavior of the End-Effector

Frequency domain and time domain methods have been used to describe the dynamic behavior of the closed-loop system. Section 6.3.1 is devoted to verifying experimentally the model of the end-point compliancy in both directions when an H is designed to close the loop as shown in Figure 10.

6.2.1 The End Point Compliancy

The nature of compliancy for the end effector is given by equation 8. H was chosen such that $(S+H)^{-1}$ in each direction is equal to the desired stiffness given by equation 5. H must also guarantee the stability of the closed-loop system. The very simplified stability criteria for a single input single output system (11) is given by inequality 9.

$$|GH| < |S + 1/E| \qquad \text{for all } \omega \in \{0,\infty\} \qquad (9)$$

1/E is very small for a very rigid environment and G is approximately equal to unity within its bandwidth. The

values for H along the normal and tangential directions within their bandwidths are 0.01 in/lbf and 0.194 in/lbf respectively. These values result in 0.39 in/lbf and 0.7 in/lbf for (S+H) within the bandwidth of the system. The values of (S+H) within its bandwidth represent the members of matrix K^{-1} in equation 5. Figure 14 shows the experimental and theoretical values of the end-point compliancy (Figure 14 actually shows the end-point admittance where it is reciprocal of the impedance in the linear case.) The experimental set-up shown in Figure 12 was used to measure the end-point compliancy. The dynamic behavior of Figure 14 can be compared with the desired dynamic response for deburring given by Figure 5.

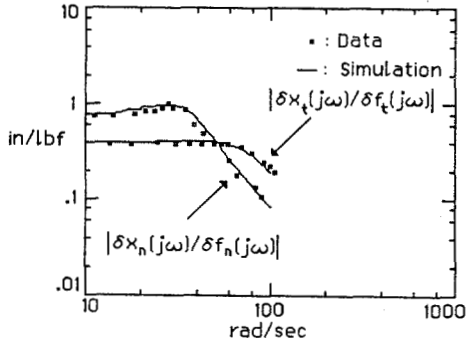

Figure 14 : The End-Point Admittance (1/Impedance)

6.2.2 Uncoupling of the Contact Forces

In this set of experiments, the whole end-effector was moved in two different directions to encounter a edge of a part. The objective was to observe the uncoupled time-domain dynamic behavior of the end-effector when the end-effector is in contact with the hard environment. The controller was designed according to reference (11) such that K_t and K_n are 0.32 lbf/in and 4.0 lb/in respectively. First the end-effector was moved 0.5" beyond the edge of the part in X_n-direction. Figure 7 shows the schematics of the experimental set-up.

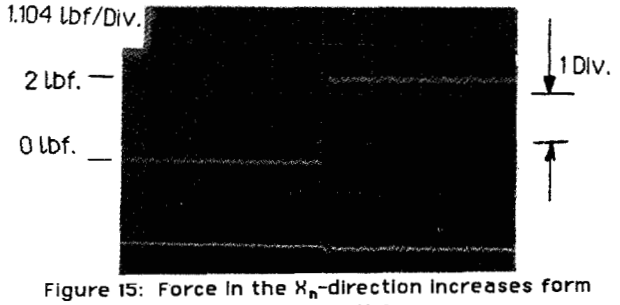

Figure 15: Force in the X_n-direction increases form zero to 2 lbf.

Figure 15 shows the contact forces. The force in X_n-direction increases from zero to 2.0 lbf while the force in the X_t-direction remains at zero. Next the end-effector was moved 0.5" beyond the edge of the part in the X_t-direction. Figure 16 shows the contact forces. The force in X_t-direction increases from zero to 0.16 lbf while the force in X_n-direction remains at zero. In both cases the end-effector was moved as 0.5" beyond the the edge of the stiff wall. Since the stiffness of the end-effector in X_n-direction is larger than the stiffness in X_t-direction, the contact force in X_n-direction is larger than the contact force in X_t-direction.

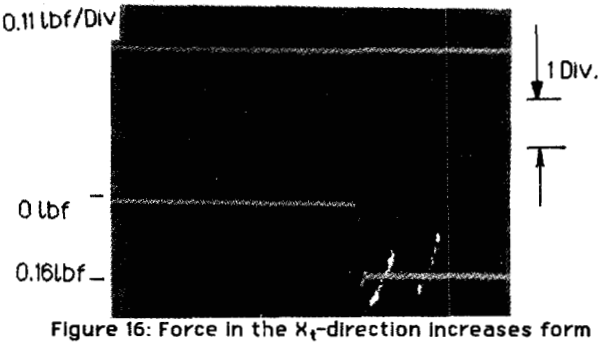

Figure 16: Force in the X_t-direction increases form zero to 0.16 lb.

6.3.3 Uncoupling of the Motion

The objective was to observe the uncoupled dynamic behavior of the end-effector in unconstrained maneuvering of the end-effector when equation 4 is satisfied. The end-point of the end-effector was commanded to move in X_t-direction. Figure 17 shows the joint angles, θ_1 and θ_4, of the end-effector when θ_1 is accepting a step-wise motion command. θ_4 remains at 180°. The plot shows the uncoupling of the joint angles in the closed-loop system.

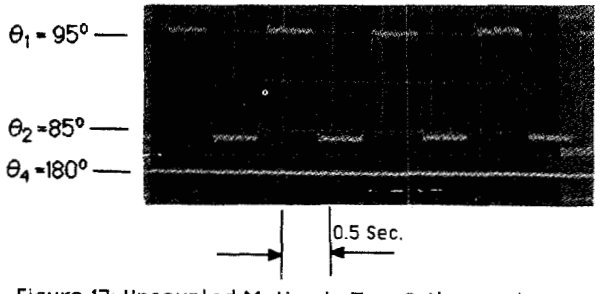

Figure 17: Uncoupled Motion in Two Orthogonal Directions

7. Summary and Conclusion

An active end-effector with controllable, compliant motion (Electronic Compliancy) has been designed, built, and tested for robotic operations. The active end-effector (unlike the passive system) does not contain any spring or dampers. The compliancy in the active end-effector is developed electronically and therefore can be modulated by an on-line computer. The active end-effector allows for compensation of the robot's position uncertainties from fixturing errors, robot programing resolution, and robot oscillations. This fully instrumented end-effector weighs only 5.05 lbs. and can be mounted at the end-point of the commercial robot manipulator. Two state-of-the-art miniature actuators power the end-effector directly. The high stiffness and light weight of the material used in the system allows for a wide bandwidth Impedance Control. A miniature force cell measures the forces in two dimensions. The tool holder can maneuver a very light pneumatic grinder in a linear work-space of about 0.3"x0.3". The measurements taken on the mechanism are contact forces, angular velocities, and the orientation of the mechanism. Satisfying a kinematic constraint for this end-effector allows for uncoupled dynamic behavior for a bounded range.

Appendix A

This appendix is dedicated to deriving of the Jacobian and the mass matrix of a general five-bar linkage. In Figure A1, j_i , l_i , x_i , m_i and θ_i represent the moment of the inertia relative to the end-point, length, location of the center of mass, mass and the orientation of each link for i= 1,2,3 and 4.

Using the standard method in (1,2), the Jacobian of the linkage can be represented by equation A1.

$$J_c = \begin{bmatrix} J_{11} & J_{12} \\ J_{21} & J_{22} \end{bmatrix} \qquad \text{(A1)}$$

where:

$J_{11} = -l_1 \sin(\Theta_1) + a\, l_5 \sin(\Theta_2)$
$J_{21} = l_1 \cos(\Theta_1) - a\, l_5 \cos(\Theta_2)$
$J_{12} = -b\, l_5 \sin(\Theta_2)$
$J_{22} = b\, l_5 \cos(\Theta_2)$

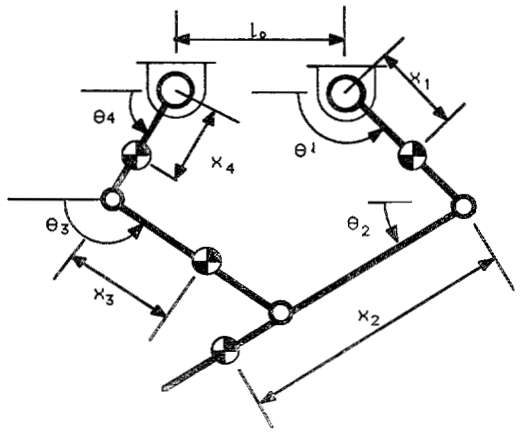

Figure A1: The Five Bar Linkage in the General Form

The mass matrix is given by equation A2.

$$M = \begin{bmatrix} M_{11} & M_{12} \\ M_{21} & M_{22} \end{bmatrix} \qquad \text{(A2)}$$

Where:

$M_{11} = j_1 + m_2 l_1^2 + j_2 a^2 + j_3 c^2 + 2 x_2 l_1 \cos(\Theta_1 - \Theta_2)\, a\, m_2$
$M_{12} = j_2 a b + b \cos(\Theta_1 - \Theta_2)\, x_2 l_1 m_2 + j_3 cd + c \cos(\Theta_4 - \Theta_3)\, x_3 l_4 m_3$
$M_{21} = M_{12}$
$M_{22} = 2 m_3 l_4 x_3 d \cos(\Theta_4 - \Theta_3) + j_3 d^2 + j_4 + m_3 l_4^2 + j_2 b^2$

a, b , c , d are given below.

$a = l_1 \sin(\Theta_1 - \Theta_3) / \{ l_2 \sin(\Theta_2 - \Theta_3) \}$
$b = l_4 \sin(\Theta_4 - \Theta_3) / \{ l_2 \sin(\Theta_2 - \Theta_3) \}$
$c = l_1 \sin(\Theta_1 - \Theta_2) / \{ l_3 \sin(\Theta_2 - \Theta_3) \}$
$d = l_4 \sin(\Theta_4 - \Theta_2) / \{ l_3 \sin(\Theta_2 - \Theta_3) \}$

References

1) Asada, H., Slotine, J. J. E., "Robot Analysis and Control", John Wiley and Sons.

2) Bausch, J., Kramer, B., Kazerooni, H., "The Development of the Compliant Tool Holders for Robotic Deburring", ASME Winter Annual Meeting, December 1986, Anaheim, California.

3) Drake, S. H., "Using Compliance in Lieu of Sensory Feedback for Automatic Assembly", IFAC Symposium of Information and Control Problems in Manufacturing Technology, Tokyo, 1977.

4) Hogan, N., "Impedance Control: An Approach to Manipulation, Part 1: Theory, Part 2: Implementation, Part 3: Applications", ASME Journal of Dynamic Systems, Measurement, and Control, 1985.

5) Hollis, R. L., "A Planar XY Robotic Fine Positioning Device", In proceedings of the IEEE International Conference on Robotics and Automation, Raleigh, North Carolina, April 1987.

6) Kazerooni, H., Houpt, P. K., Sheridan, T. B., "Fundamentals of Robust Compliant Motion for Manipulators" ,IEEE Journal of Robotics and Automation , N2, V2, June 1986.

7) Kazerooni, H., Houpt, P. K., Sheridan, T. B., "A Design Method for Robust Compliant Motion of Manipulators", IEEE Journal of Robotics and Automation .N2, V2, June 1986.

8) Kazerooni, H., Bausch, J. J., Kramer, B., "An Approach to Automated Deburring by Robot Manipulators", ASME Journal of Dynamic Systems, Measurements and Control, December 1986.

9) Kazerooni, H., Bausch, J. J., Kramer, B., "An approach to Robotic Deburring" , In proceeding of American Control Conference , Seattle, June 86.

10) Kazerooni, H., "Automated Robotic Deburring Using Electronic Compliancy; Impedance Control", In proceedings of the IEEE International Conference on Robotics and Automation, Raleigh, North Carolina, March 1987.

11) Kazerooni, H., " Non-linear Robust Impedance Control for Robot Manipulators", In proceedings of the IEEE International Conference on Robotics and Automation, Raleigh, North Carolina, April 1987.

12) Rappaport, S. "Five-bar Linkage for Straight Line Motion", Product Engineering, October 1959.

13) Raibert, M. H., Craig, J. J., "Hybrid Position/Force Control of Manipulators", ASME Journal of Dynamic Systems, Measurement, and Control.

14) Slotine, J. J. , "Sliding Controller Design for Non-linear Systems", International Journal of Control, V40, N2, 84.

15) Slotine, J. J., "The robust Control of of Robot Manipulators", The international Journal of Robotics Research, V4, N2, 1985.

16) Vidyasagar, M., "Non-linear Systems Analysis", Prentice-Hall.

17) Vidyasagar, M., Desoer, C. A., "Feedback Systems: Input-Output Properties", Academic Press.

18) Vidyasagar, M., Spong, M. W., "Robust Non-linear Control of Robot Manipulators", IEEE Conference on Decision and Control", December 1985.

19) Yoshikawa, T., "Dynamic Manipulability of Robot Manipulators", Journal of Robotic Systems, Volume 2, Number 1, 1985.

20) Watson, P. C.,"A Multidimensional System Analysis of the Assembly Process as Performed by a Manipulator", In Proceedings of the First American Robot Conference, Chicago, 1976.

21) Whitney, D. E., "Force-Feedback Control of Manipulator Fine Motions", ASME Journal of Dynamic Systems, Measurement, and Control June, 1977.

This research is partially supported by NSF grant, under contract number NSF/DMC 8604123.